A coupled near and far wake model for wind turbine aerodynamics

Pirrung, Georg R.; Aagaard Madsen , Helge; Kim, Taeseong; Heinz, Joachim Christian

Published in:
Wind Energy

Link to article, DOI:
10.1002/we.1969

Publication date:
2016

Document Version
Publisher's PDF, also known as Version of record

Wind Energy

WIND ENERGY
Wind Energ. (2016)
Published online in Wiley Online Library (wileyonlinelibrary.com). DOI: 10.1002/we.1969

RESEARCH ARTICLE

A coupled near and far wake model for wind turbine aerodynamics

G. R. Pirrung, H. A. Madsen, T. Kim and J. Heinz

Wind Energy Department, Technical University of Denmark, Frederiksborgvej 399, Building 118, Roskilde, DK-4000, Denmark

ABSTRACT

In this paper, an aerodynamic model consisting of a lifting line-based trailed vorticity model and a blade element momentum (BEM) model is described. The focus is on the trailed vorticity model, which is based on the near wake model (NWM) by Beddoes and has been extended to include the effects of downwind convection and to enable a faster and more accurate computation of the induction, especially close to the blade root and tip. The NWM is introduced to model the detailed steady and unsteady induction from the first part of the trailed vorticity behind the individual rotor blades. The model adds a radial coupling between the blade sections and provides a computation of tip loss effects that depends on the actual blade geometry and the respective operating point. Moreover, the coupling of the NWM with a BEM theory-based far wake model is presented. To avoid accounting for the near wake induction twice, the induction from the BEM model is reduced by a coupling factor, which is continuously updated during the computation to ensure a good behavior of the model in varying operating conditions. The coupled near and far wake model is compared with a simple prescribed wake lifting line model, a BEM model and full rotor computational fluid dynamics (CFD) to evaluate the steady-state results in different cases. The model is shown to deliver good results across the whole operation range of the NREL 5-MW reference wind turbine. ©2016 The Authors Wind Energy Published by John Wiley & Sons Ltd.

KEYWORDS
blade element momentum; lifting line; near wake model; rotor aerodynamics

Correspondence
G. R. Pirrung, Wind Energy Department, Technical University of Denmark, Frederiksborgvej 399, Building 118, Roskilde, DK-4000, Denmark.
E-mail: gepir@dtu.dk

Received 3 September 2014; Revised 11 August 2015; Accepted 13 January 2016

1. INTRODUCTION

The aerodynamic computations in most aeroelastic wind turbine codes are based on blade element momentum (BEM) theory, where the blade is divided into radial sections and the blade forces are equated with the forces acting on the wind by an annular element of the actuator disk through which the rotor is represented. This approach leads to good results if the BEM model is extended by a tip loss correction factor to take into account the finite number of blades,[1] a dynamic inflow model to include the inertia of the wake[2] and further extensions to cover e.g. sheared inflow and yaw error. The main advantage of a BEM model compared with other, more advanced, aerodynamic models, such as vortex codes and CFD[3] is the very fast computation time while obtaining good results in normal operation cases.

A major shortcoming of the BEM model is that it does not provide flow details close to the individual rotor blades. It is therefore common in BEM-based aeroelastic codes to use a sub-model to compute the influence of the shed vorticity (Theodorsen effect) behind the individual blades. The shed vorticity only influences the unsteady induction and does not alter the steady loading of the wind turbine. Shed vorticity effects are of big importance for computation of unsteady loading, e.g. in the case of flutter computations.[4] The induction effects due to trailed vorticity, on the other hand, are commonly modeled by a tip loss correction, but such a correction only captures the effects of the tip vortex in steady conditions. It has therefore been proposed to model the trailed vorticity in the vicinity of the blades with a sub-model[5,6] in order to improve the unsteady computation of the details of the induction at the blade. Trailed vorticity close to the blade covers, opposed to shed vorticity, a large part of the steady-state induced velocities because of the wind turbine wake.

Therefore, the implementation of a trailed vorticity model in a fast, BEM-based aerodynamics model is more complex than the implementation of a shed vorticity model, and care has to be taken to ensure adequate steady-state computations.

This paper presents further development of a coupled aerodynamics model consisting of a BEM model for the far wake computation and a lifting line-based trailed vorticity model, the so-called near wake model (NWM) developed by Beddoes.[5] This coupled aerodynamics model has been proposed by Madsen and Rasmussen for application on wind turbines,[6] and promising results have been obtained by Andersen.[7] The purpose of the NWM part is to account for both the root and tip vortices, to add an aerodynamic coupling between the radial sections along the blade span and to provide a more accurate modeling of the near wake induction dynamics. The BEM model is necessary to compute the induction from the far wake and the slower dynamic inflow effects that are not due to trailed vorticity in vicinity of the blades but linked to integral load changes on the rotor disk.

The NWM originally assumes the trailed vorticity to stay in the rotor plane, which is a good approximation for operation at high tip speed ratio. Above rated wind speed, the downwind convection speeds of the trailed vorticity are higher, and accordingly, the vorticity path is better approximated by helices. Wang and Coton[8] proposed to include the helix angle in the NWM but did not account for the decreasing induction because of the larger distance between the trailed vorticity and the blade when the vorticity has convected downwind. This increased distance is mainly important close to the blade root, where the root vortex is trailed at a large helix angle, and is accounted for by the model presented in this paper.

Moreover, the basic assumption of the NWM, stating that the induction due to the trailed vorticity approaches zero within a quarter revolution, is not valid for the induction at the blade root because of the tip vortex, which is shown in Section 4.2. There, a correction is presented that limits the near wake induction in this case to the induction from a quarter revolution to avoid an overestimation of induced velocities.

A disadvantage of previous implementations of the coupled aerodynamics model has been that the coupling factor, which is used to reduce the full BEM induction to account for the part of the induction that is included in the NWM, had to be calculated before the simulations.[7] In the present implementation, the coupling factor is adjusted during the computation to match the steady-state thrust of a BEM model. This approach ensures that the mean induction results are similar to the well-validated BEM method, while different radial induction distributions due to, e.g. trailed vorticity at trailing edge flaps or a partial pitch blade, can be modeled. Also, the dynamic behavior of the induction due to trailed vorticity is retained in the model.

To evaluate the coupled aerodynamic model, the results are compared with the BEM model implemented in HAWC2 and full rotor CFD results from EllipSys3D.[3] The focus in this paper is on the steady-state results, i.e. on the handling of near and far wake by different models, on the coupling factor computation and on the effectiveness of the root and convection corrections. Evaluating the improvement of the unsteady aerodynamic response due to the trailed vorticity computation, which is the main benefit of introducing the NWM, falls outside the scope of this paper.

The following section will present the NWM as described by Beddoes,[5] improved by Wang and Coton[8] and implemented in a coupled near and far wake model for rotor aerodynamics by Madsen and Rasmussen[6] and Andersen.[7] Section 3 is a brief analytical derivation of the induction from helical vortex arcs, which will be used to correct for the error due to neglecting the downwind convection and further to analyze the axial and tangential induction from the near wake of one blade and the induction due to the remaining trailed wake of a three-bladed rotor. In Section 4, modifications of the NWM to improve accuracy and computation speed are presented. Section 5 discusses the implementation in a coupled near and far wake model, where the coupling factor is computed and modified during the simulation. Results are shown in Section 6, where the coupled model is compared with numerical integration of the Biot–Savart law, a BEM model and full rotor CFD.

2. ORIGINAL MODEL DESCRIPTION

2.1. Near wake model

The purpose of the NWM is to approximate the induction at a blade because of the vorticity trailed from that blade in a quarter of a rotor revolution. To make an efficient computation possible, Beddoes[5] assumes that the trailed vorticity follows prescribed circular arcs in the rotor plane. Using the Biot–Savart law, the axial induction dw from a vortex element with the length ds on a circular arc trailed at radius r at a point on the blade at a distance h from the vortex trailing point, compared with Figure 1, can be found as

$$dw = \frac{\Delta\Gamma ds}{4\pi r^2} \frac{1 - \left(1 - \frac{h}{r}\right)\cos(\beta)}{\left[1 + \left(1 - \frac{h}{r}\right)^2 - 2\left(1 - \frac{h}{r}\right)\cos(\beta)\right]^{3/2}} \tag{1}$$

where $\beta = \Omega t$ is the angle the blade has moved since the element has been trailed and $\Delta\Gamma$ is the vortex strength of the element. Equation (1) is derived in Section 3 for the more general case including downwind convection. To obtain the

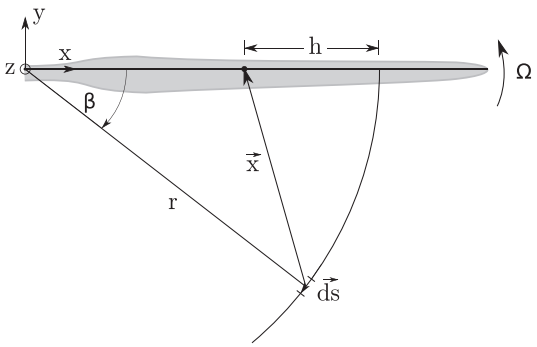

Figure 1. Sketch of the blade geometry with vorticity trailed at radius r. Since the vortex element $\vec{ds}$ has been trailed, the blade has moved by an angle β at the angular velocity Ω. The induction is to be computed at a blade section the distance h inboard from the vortex trailing point.

induction from a vortex arc, Equation (1) could be integrated numerically. But it is very computationally expensive to obtain the induction from the trailed wake along the blade in this way: If the blade is discretized into n sections and $n+1$ vortices are trailed at the root and tip of the blade and in between the sections, $n(n+1)$ integrations of Equation (1) are necessary to obtain the induction because of every trailed vortex arc at every blade section. This amount of additional computations would slow down an aeroelastic wind turbine code considerably, where the BEM-based aerodynamics usually are much faster than the structural part.

A fast trailing wake algorithm has been developed by Beddoes to speed up these integrations. The basic idea is to compute the induction from a vortex element at the lifting line ($\beta = 0$) and let that value decrease as the blade rotates away from that element. This decay of the induction can then be efficiently computed using exponential functions. The induction from an element at the lifting line follows directly from equation (1):

$$dw_0 = dw(\beta = 0) = \frac{\Delta\Gamma ds}{4\pi r^2} \frac{1 - \left(1 - \frac{h}{r}\right)}{\left[1 + \left(1 - \frac{h}{r}\right)^2 - 2\left(1 - \frac{h}{r}\right)\right]^{3/2}} = \frac{\Delta\Gamma r d\beta}{4\pi h|h|} \tag{2}$$

Beddoes proposed to use this induction value at the lifting line dw_0 to make the induction from an element at the position β, Equation (1), dimensionless. This results in a spatial decay function dw/dw_0, which starts at the value 1 and then decreases for increasing β. Beddoes proposed to approximate this function by exponential functions:

$$\frac{dw}{dw_0} = \frac{\left(\frac{h}{r}\right)^2 \left[1 - \left(1 - \frac{h}{r}\right)\cos(\beta)\right]}{\left[1 + \left(1 - \frac{h}{r}\right)^2 - 2\left(1 - \frac{h}{r}\right)\cos(\beta)\right]^{3/2}} \approx 1.359e^{-\beta/\Phi} - 0.359e^{-4\beta/\Phi} \tag{3}$$

where Φ is a geometrical factor depending on r and h. In this paper, an improved expression for Φ by Wang and Coton[8] is used. This definition leads to a reduced error if the vortices are trailed further inboard than the blade section where the induction shall be computed, which is defined as $h/r < 0$.

$$\Phi = \frac{\pi}{4}\left|\left(1 + \frac{h}{2r}\right)\ln\left(1 - \frac{h}{r}\right)\right| \qquad \text{for } 0 < h/r < 1 \tag{4a}$$

$$\Phi = \frac{1 - \frac{h}{r}}{1.5 + \ln\left(1 - \frac{h}{2r}\right)} \qquad \text{for } h/r < 0 \tag{4b}$$

In Sections 4.2 and 4.3, Φ is further modified to improve the accuracy of the induction at the inboard part of the blade because of vortices close to the tip, i.e. $h/r \to 1$, and to model the downwind convection of the trailed vorticity.

The trailing wake algorithm proposed by Beddoes determines the near wake induction W at a point on the blade at a given time step i as

$$W^i = X_w^i + Y_w^i \tag{5}$$

with a slowly decaying component X_w and a faster decaying component Y_w, which accumulate the history of the near wake development. The values of these components depend both on their values at the preceding time steps, which have decreased exponentially, and the new contributions D_w from the vortex element trailed at the current step:

$$X_w^i = X_w^{i-1} e^{-\Delta\beta/\Phi} + 1.359 D_w e^{-\Delta\beta/2\Phi} \tag{6a}$$

$$Y_w^i = Y_w^{i-1} e^{-4\Delta\beta/\Phi} - 0.359 D_w e^{-2\Delta\beta/\Phi} \tag{6b}$$

where Beddoes defined $\Delta\beta = \Omega\Delta t$ as the blade movement during a time step. For the computations in this paper, the wake rotation, represented by tangential induction, is included, defining $\Delta\beta = (v_y/r)\Delta t$, where v_y denotes the in-plane component of the relative velocity. Assuming a straight element perpendicular to the lifting line and applying the Biot–Savart law, the induction D_w due to the new element trailed during the time step is found as

$$D_w = \frac{\Delta\Gamma\left(\frac{\Delta s}{|h|}\right)}{4\pi h\left[1 + \left(\frac{\Delta s}{h}\right)^2\right]^{1/2}} \tag{7}$$

where Δs is the length of the element. Exponential functions evaluated at half a time step are used to determine the fractions of D_w driving the faster and slower decaying parts of the induction in Equations (6). The resulting fractions of D_w are added to the decreased contributions from all previous components included in X_w^{i-1} and Y_w^{i-1}.

To account for the movement of the vortices out of the rotor plane in the presence of downwind convection, Wang and Coton[8] introduced the angle φ of the helix formed by the trailed vortex filaments in the calculation of D_w. Andersen[7] proposed to also include the tangential induction in a similar way:

$$D_{w,z} = D_w \cos(\varphi) \quad \text{and} \tag{8}$$

$$D_{w,y} = D_w \sin(\varphi) \tag{9}$$

The subscripts z and y denote the axial and tangential induction, respectively. The values for the induction from the first element are then inserted in Equations (6) replacing D_w. Thus, Equations (5) and (6) have to be solved for both axial and tangential induction.

2.2. Coupling to far wake model

The NWM is only accounting for the induction because of the trailed vorticity in the first quarter of a rotation. A model for rotor aerodynamics must therefore include a far wake model and a shed vorticity model to cover the complete induction from the rotor. As in previous implementations,[6,7] a BEM model with reduced thrust is used to model the far wake. The shed vorticity model used in this paper is based on the inviscid part of the Beddoes–Leishman-type model by Hansen *et al*.[9]

The BEM model used for the far wake includes a dynamic inflow model with two different time constants, as in the aeroelastic code HAWC2.[10–12] No tip loss effects are included in the far wake model, because they are taken care of by the NWM (cf. Section 6.1.3). In this paper, only uniform inflow without turbulence is considered; therefore, it is unnecessary to compute the induction on a grid to account for, e.g. wind shear and independent motion of individual blades, as in HAWC2. Instead, the far wake induction is assumed to be constant on each annular element of the rotor.

In the BEM model, first, the aerodynamic forces are computed. To account for the part of the thrust included in the NWM, the thrust coefficient is then reduced by multiplying with a coupling factor k_{FW}:

$$C_{T,FW} = C_T k_{FW} \tag{10}$$

The induction follows from the thrust coefficient based on the following polynomial function,[2] which is used in the HAWC2 BEM model:

$$a_{FW,QS} = k_3 C_{T,FW}^3 + k_2 C_{T,FW}^2 + k_1 C_{T,FW} + k_0 \tag{11}$$

In the previous implementations, the coupling factor was provided as an input by the user and had to be calculated in preceding simulations, with a goal to achieve the same mean induction as in a BEM model.[7] A method to determine the coupling factor during the computation is described in Section 5, so that no additional input for the NWM is needed and the rotor thrust matches the one obtained from a BEM model in steady computations.

3. INDUCTION FROM HELICAL VORTEX ARCS

In this section, the basic NWM equations are derived for axial and tangential induction including out-of-plane movement of the vortex filaments with a constant downwind convection velocity. The goal is to obtain a basis for evaluating the induction computed by the NWM and for developing a convection correction in Section 4.3. A constant downwind convection velocity v_h results in helical instead of circular vortex arcs. The helix angle φ, with $\tan\varphi = v_h/(\Omega r)$, depends on the radial position of the vortex trailing point. The following derivations are based on the geometry sketched in Figure 1. The vortex is trailed at a blade radius r; the induction is to be calculated at a blade section at the distance h from the origin of the vortex. The vector $\vec{x}$ points from the location of the trailed vortex filament to the blade section, and the filament $\vec{ds}$ is pointing away from the blade. The x-axis points from blade root to blade tip, the y-axis in front of the blade, away from the trailed vorticity, and the z-axis is positive upwind.

In terms of r, β and h, $\vec{x}$ and $\vec{ds}$ are expressed as follows:

$$\vec{x} = \begin{pmatrix} -r\cos\beta + r - h \\ r\sin\beta \\ v_h\beta/\Omega \end{pmatrix}, \quad \vec{ds} = \frac{ds}{\sqrt{1+\left(\frac{v_h}{\Omega r}\right)^2}} \begin{pmatrix} -\sin\beta \\ -\cos\beta \\ -v_h/(\Omega r) \end{pmatrix} \tag{12}$$

The Biot–Savart law gives for the induction due to this filament at the blade section

$$\vec{dw} = \frac{\Gamma}{4\pi}\frac{\vec{x}\times\vec{ds}}{|\vec{x}|^3} \tag{13}$$

The z-component, the axial induction, is evaluated as

$$\begin{aligned} dw_z &= \frac{\Gamma}{4\pi}\frac{x_x ds_y - x_y ds_x}{|\vec{x}|^3} \\ &= \frac{\Gamma ds\cos\varphi}{4\pi r^2}\frac{1-\left(1-\frac{h}{r}\right)\cos\beta}{\left(1+\left(1-\frac{h}{r}\right)^2 - 2\left(1-\frac{h}{r}\right)\cos\beta + \left(\frac{v_h\beta}{\Omega r}\right)^2\right)^{3/2}} \end{aligned} \tag{14}$$

where φ is the helix angle

$$\cos\varphi = \frac{\Omega r}{\sqrt{(\Omega r)^2 + v_h^2}} = \frac{1}{\sqrt{1+\left(\frac{v_h}{\Omega r}\right)^2}} \tag{15}$$

The axial induction from a filament of finite length at the blade, i.e. $\beta = 0$, can be found as

$$dw_{0,z} = \frac{\Delta\Gamma ds\cos\varphi}{4\pi h|h|} \tag{16}$$

This leads to the following equation for axial induction, which includes downwind convection:

$$\frac{dw_z}{dw_{0,z}} = \frac{\left(\frac{h}{r}\right)^2\left[1-\left(1-\frac{h}{r}\right)\cos\beta\right]}{\left(1+\left(1-\frac{h}{r}\right)^2 - 2\left(1-\frac{h}{r}\right)\cos\beta + \left(\frac{v_h\beta}{\Omega r}\right)^2\right)^{3/2}} \tag{17}$$

Equations (14) and (16) are obtained for vortices that convect downwind with a constant speed depending on the wind speed at the rotor plane. These equations contain two terms that are additions to the equations without convection, $\cos\varphi$ and $((v_h\beta)/(\Omega r))^2$. The only difference between Equations (17) and (3) is the term $((v_h\beta)/(\Omega r))^2$, which describes the increasing distance from vortex trailing point to calculation point because of the downwind convection.

The equation for the induced velocity in the rotor plane perpendicular to the blade can be derived similarly to the axial velocity. It is the y-component of Equation (13). The induction from the first element is the $\sin\varphi$ counterpart of Equation (16). That leads to the spatial decay function for tangential induction:

$$\frac{dw_y}{dw_{0,y}} = \frac{\left(\frac{h}{r}\right)^2\left(1-\frac{h}{r}-\cos\beta-\beta\sin\beta\right)}{\left(1+\left(1-\frac{h}{r}\right)^2 - 2\left(1-\frac{h}{r}\right)\cos\beta + \left(\frac{v_h\beta}{\Omega r}\right)^2\right)^{3/2}} \tag{18}$$

The inductions computed using Equations (17) and (18) differ for not small β and h/r. This is because the angle of the in-plane induction changes as β increases and so does the fraction of the induction that is perpendicular to the blade and contributes to the velocity triangle. There is also an in-plane component of the induction because of the vorticity parallel to the rotor plane that increases as the vorticity convects downstream. Thus, using the same approximation, Equation (3) for tangential induction as for axial induction, as proposed by Andersen,[7] introduces an error. This error is quantified in Section 4.3.

Assuming a constant downwind convection velocity and no wake expansion, Equations (16)–(18) can be used as a basis for computing the induction due to the trailed wake of a three-bladed rotor. To model blades at different positions, an angle β_{start} is added, which is 0 for the blade where the induction shall be calculated, 120° for the blade behind in the direction of rotation and −120° for the blade in front. The axial induction from a quarter rotation at the blade is then given as

$$W = \sum_{i=1}^{3} W_i, \quad \text{where} \tag{19}$$

$$W_i = \frac{dw_0}{d\beta} \int_{\beta_{start,i}}^{\pi/2+\beta_{start,i}} \frac{dw}{dw_0}\, d\beta \tag{20}$$

To obtain the induction due to the wake trailed from the other blades, the z-component of $\vec{x}$, Equation (12), has to be modified so that the trailed vorticity starts in the rotor plane for $\beta = \beta_{start}$, resulting in $x_z = v_h(\beta - \beta_{start})/\Omega$, thus following for the axial and tangential induction

$$\frac{dw_z}{dw_{0,z}} = \frac{\left(\frac{h}{r}\right)^2 \left[1 - \left(1 - \frac{h}{r}\right)\cos\beta\right]}{\left(1 + \left(1 - \frac{h}{r}\right)^2 - 2\left(1 - \frac{h}{r}\right)\cos\beta + \left(\frac{v_h(\beta-\beta_{start})}{\Omega r}\right)^2\right)^{3/2}} \tag{21}$$

$$\frac{dw_y}{dw_{0,y}} = \frac{\left(\frac{h}{r}\right)^2 \left(1 - \frac{h}{r} - \cos\beta - (\beta - \beta_{start})\sin\beta\right)}{\left(1 + \left(1 - \frac{h}{r}\right)^2 - 2\left(1 - \frac{h}{r}\right)\cos\beta + \left(\frac{v_h(\beta-\beta_{start})}{\Omega r}\right)^2\right)^{3/2}} \tag{22}$$

This formulation can be used to compute the far wake as well, by integrating Equation (20) from $\pi/2 + \beta_{start,i}$ to infinity or, in practice, a sufficiently high number of rotations, e.g. 32π.

Further, the equations shown recently can be used to calculate the induction from a steady trailed wake without wake expansion and a constant convection speed for a blade discretized in calculation points and vortex trailing points. It can serve as a reference for comparison with the NWM and to evaluate the division of the wake into a near wake and a far wake based on BEM computations. The input, namely, axial and tangential induction, to determine v_h and vortex strength, can be obtained by using the coupled near and far wake model. In order to obtain a reasonable result from the helical vortex model for the far wake, the downstream convection velocity is limited to a minimum of $2/3v_\infty$. This limit on the convection can be justified because, especially close to the tip of the blade, the induction is a function of the azimuth angle, with a much higher induction at a blade than in between blades. Thus, having the tip vortex convect with $v_h = v_\infty - v_{ax,tip}$ would lead to an overestimated far wake induction, because the tip vortex stays close to the rotor plane for many revolutions. The minimum convection speed is relevant at wind speeds below rated.

4. NEAR WAKE MODEL MODIFICATIONS

4.1. Modified trailing functions

The original approach of first calculating the induction D_w from a finite length element and a subsequent splitting in two components, Equation (6), has a major disadvantage. For time steps of 0.01 or 0.02 s and cosine-based spatial discretization of 30 to 60 points, which are widely used in aeroelastic wind turbine codes, for example in the HAWC2 models available online,[13] the induction from the newest element can be drastically underestimated close to the root and tip of the blade. The reason for this is in the splitting of D_w into X_w and Y_w using exponential functions that are evaluated at half a time step [cf. Equation (6)].

The starting point for the development of an improved approach is Equation (2). Division by $d\beta$ leads to

$$\frac{dw_0}{d\beta} = \Delta\Gamma \frac{r}{4\pi h|h|} \tag{23}$$

The induction from the newest element, which in the original model is assumed to be a straight element, see Equation (7), can instead be computed as

$$\begin{aligned} D_w &= \frac{dw_0}{d\beta}\Delta\beta\left\langle\frac{dw}{dw_0}\right\rangle \\ &= \Delta\Gamma\frac{r}{4\pi h|h|}\int_0^{\Delta\beta}\frac{dw}{dw_0}\,d\beta \end{aligned} \tag{24}$$

Here, a constant induction along the element $(dw_0/d\beta)\Delta\beta$ is corrected by multiplying with the decay function dw/dw_0 averaged over the length of the element. Inserting Equation (3) yields

$$\begin{aligned} D_w &= \Delta\Gamma\frac{r}{4\pi h|h|}\int_0^{\Delta\beta}\left(1.359e^{-\beta/\Phi}-0.359e^{-4\beta/\Phi}\right)d\beta \\ &= \Delta\Gamma\frac{r}{4\pi h|h|}\Phi\left[1.359\left(1-e^{-\Delta\beta/\Phi}\right)-\frac{0.359}{4}\left(1-e^{-4\Delta\beta/\Phi}\right)\right] \\ &\equiv \Delta\Gamma\left[D_X\left(1-e^{-\Delta\beta/\Phi}\right)+D_Y\left(1-e^{-4\Delta\beta/\Phi}\right)\right] \end{aligned} \tag{25}$$

Now, the induction of the first element is divided into slow and fast decaying components, which can be directly inserted into Equation (6):

$$W_i = X_w^i + Y_w^i \tag{26a}$$

$$X_w^i = X_w^{i-1}e^{-\Delta\beta/\Phi} + D_X\Delta\Gamma\left(1-e^{-\Delta\beta/\Phi}\right) \tag{26b}$$

$$Y_w^i = Y_w^{i-1}e^{-4\Delta\beta/\Phi} + D_Y\Delta\Gamma\left(1-e^{-4\Delta\beta/\Phi}\right) \tag{26c}$$

In this formulation, the error in evaluating the trailing functions does not depend on the time step and the spatial point density, since D_w is split into an X_w and Y_w component according to Beddoes' exponential approximation, Equation (3). Because Equation (3) approximates the induction due to a curved vortex arc, the approach presented in Equation (25) makes the assumption of a straight first element, as in Equation (7), unnecessary.

The new expression for D_w is based on an integration over the angle β, which is defined in the rotor plane, as opposed to an integration over the length of the element. Therefore, the induction from the newest element in Equation (25) is, in fact, the axial induction component. The equivalent of Equations (26) for the tangential induction can be obtained through multiplication of D_X and D_Y by $\tan\varphi$, the tangent of the helix angle.

A comparison of the original way to calculate the induction from the newest element and the proposed modification is shown in Figure 2. The X and Y components associated with D_w from Equations (6) and (26) are plotted depending on the time step for an example case with $h/r = 0.01$. The plot shows that the original evaluation is deviating from the new formulation already at small time steps. This error would have to be reduced by using smaller time steps or sub-time steps for the NWM, both options slowing down the computations.

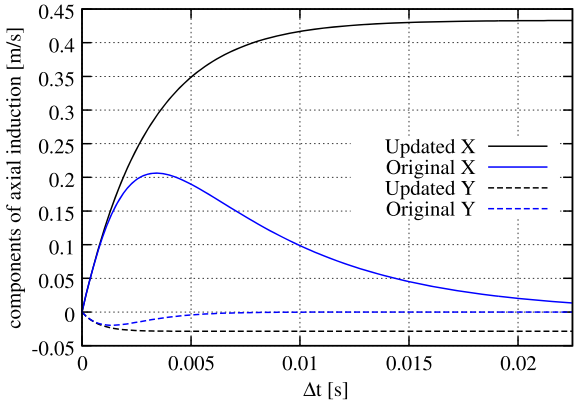

Figure 2. Comparison of the induction from the newest element, divided in the X and Y components depending on the chosen time step. The vortex with $\Delta\Gamma = 1$ is trailed from $r = 60$ m, the blade rotates with 12.1 rpm and the calculation point placed at $r = 59.4$ m, so $h/r = 0.01$.

Another advantage is that D_X and D_Y only depend on the grid point distribution along the blade span, which is constant during a simulation, and not on Δs, like the original D_w, see Equation (7). Therefore, D_X and D_Y can be computed in the initialization of the program, which, in combination with the halved number of evaluations of exponential functions in Equation (26) compared with Equation (6), greatly improves the computational speed.

4.2. Root correction

For small, positive values of h/r, which means that the vortex trailing point and the calculation point are close and the trailing point is further outboard, both the analytical spatial decay function and Beddoes' approximation, Equation (3), reach small values within the first 90 degrees (cf. Figure 3). If the calculation point moves further inboard and h/r gets closer to one, the function values decrease slower, as seen in the right plot. They do not approach zero within 90 degrees, even for higher convection speeds. Because induced velocity contributions from the newest element are constantly added to the X_w and Y_w components and old contributions are not removed, using the near wake algorithm, Equations (5) and (6) or (26), corresponds to an integration of the spatial decay function dw/dw_0, Equation (3) to infinity. Therefore, the NWM gives a higher induction than the value of a quarter circle if dw/dw_0 does not reach zero within 90 degrees.

The goals of the correction here are to limit the steady-state induction the NWM gives to that of a quarter circle and to reduce the dynamic effects afterwards.

Inserting $\Delta\beta = \pi/2$ in Equation (25) leads to the induction from a quarter circle of trailed vorticity with constant circulation according to Beddoes' functions:

$$D_{w,\pi/2} = \Delta\Gamma\left[D_X\left(1 - e^{-\pi/(2\Phi)}\right) + D_Y\left(1 - e^{-2\pi/\Phi}\right)\right] \tag{27}$$

If the NWM is applied, the following induction is reached because of the integration to infinity:

$$D_{w,\infty} = \Delta\Gamma(D_X + D_Y) \tag{28}$$

The correction factor is then found as

$$C = \frac{D_{w,\pi/2}}{D_{w,\infty}} = \frac{D_X\left(1 - e^{-\pi/(2\Phi)}\right) + D_Y\left(1 - e^{-2\pi/\Phi}\right)}{D_X + D_Y} \tag{29}$$

$$\tag{30}$$

The root correction factor is applied in the NWM by correcting Φ, which leads to corrected D_X and D_Y in the initialization of the program:

$$\Phi_C = \Phi C, \quad D_{X,C} = 1.359\frac{r}{4\pi h|h|}\Phi_C, \quad D_{Y,C} = -\frac{0.359}{4}\frac{r}{4\pi h|h|}\Phi_C \tag{31}$$

It is shown in Figure 4 how this approach limits the induction to the value reached after a quarter rotation.

The steady induction given by the integral of the exponential functions to infinity is compared with that by the integral of the analytical solution over a quarter circle in Figure 5. The root correction reduces the error of the blade root induction due to the tip vortex, ($h/r \to 1$), from over 300% to roughly 5%.

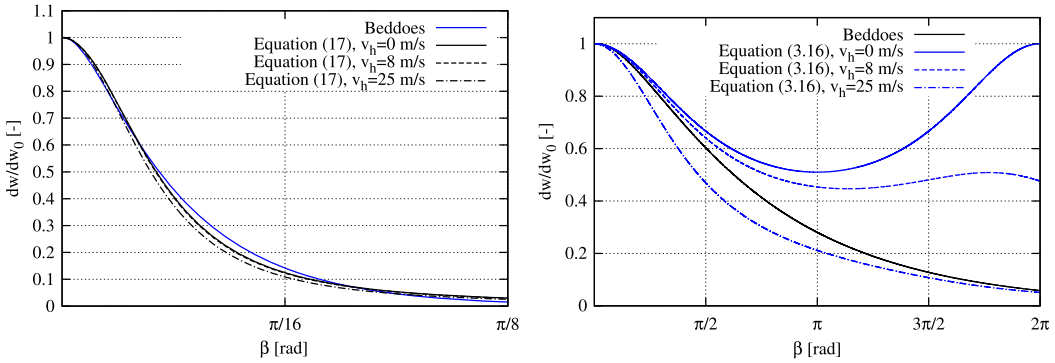

Figure 3. Comparison of the analytical trailing function, Equation (17), and Beddoes' approximation, Equation (3), for $h/r = 0.1$ (left) and $h/r = 0.8$ (right). Zero is clearly not reached within a quarter rotation at large h/r, even at high hub wind speeds.

DOI: 10.1002/we

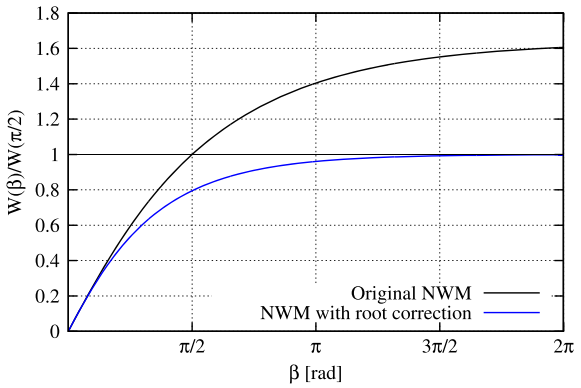

Figure 4. Induction due to constant trailed vorticity of length β as fraction of the induction due to a quarter circle at $h/r = 0.8$. The black curve shows the behavior of the original near wake model (NWM). Applying the correction factor on the value leads to the response shown in the gray curve.

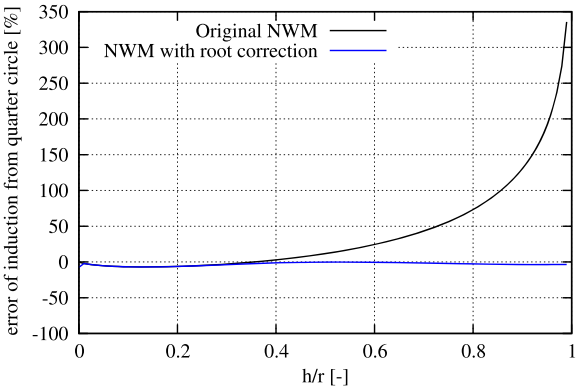

Figure 5. Integral error of original and corrected near wake model (NWM) trailing functions compared with analytical solution. The error for negative h/r has been reduced by using the Φ according to Wang and Coton; the error for positive h/r is reduced because of the new root correction.

4.3. Correction for downwind convection

The influence of the downwind convection of the vortices can be included in the NWM with the helix angle as additional parameter. This additional parameter is here included in the decay rate Φ, which is then not only a function of h/r, cf. Equation (4), but also a function of the tangent of the helix angle φ.

Wang and Coton[8] proposed to obtain an optimal value for Φ by integrating both sides of Equation (3) and numerically determining the value of Φ for which the integral of the approximation equals the integral of the Biot–Savart law. The same approach is used in this work to determine optimal values of Φ in the presence of downwind convection, where the exact solution of the induction decay is given by Equation (17). The optimal Φ for computing the axial induction solves the following equation:

$$\int_0^{pi/2} \left(\frac{\left(\frac{h}{r}\right)^2 \left[1 - \left(1 - \frac{h}{r}\right)\cos\beta\right]}{\left(1 + \left(1 - \frac{h}{r}\right)^2 - 2\left(1 - \frac{h}{r}\right)\cos\beta + \left(\frac{v_h \beta}{\Omega r}\right)^2\right)^{3/2}} \right) d\beta = \int_0^{pi/2} \left(1.359 e^{-\beta/\Phi_{opt,z}} - 0.359 e^{-4\beta/\Phi_{opt,z}}\right) d\beta \tag{32}$$

For the tangential induction computation, the optimal Φ follows accordingly from Equation (18).

To correct the Φ as proposed by Wang and Coton, Equation (4), for downwind correction, it is multiplied by a factor f. This factor approximates the ratio of $\Phi_{opt,z}(\tan\varphi \neq 0)$, the optimal Φ, if downwind convection is present, over

$\Phi_{opt,z}(\tan\varphi = 0)$, the optimal Φ for trailed vorticity that stays in the rotor plane:

$$\Phi^* = \Phi \frac{\Phi_{opt,z}(\tan\varphi \neq 0)}{\Phi_{opt,z}(\tan\varphi = 0)} \approx \Phi f(h/r, \tan\varphi) \tag{33}$$

The factor f will, as the factor C for the root correction presented in the previous section, be applied on both Φ and D_X and D_Y [cf. Equation (31)]. As opposed to C, which is computed in the initialization and depends on the discretization, f depends on the helix angle and thus has to be updated during the computations. It has been obtained through curve fitting as

$$f = (1.1e^{-b_1(h/r)\tan\varphi} + a_2(h/r)e^{-b_2(h/r)\tan\varphi} - 0.1 - a_2(h/r)) \tag{34}$$

The dependency of the parameters b_1, a_2, b_2 on h/r has been as well approximated by exponential functions:

$$b_1 = a_{1,1} + a_{1,2}e^{a_{1,3}h/r} + a_{1,4}e^{a_{1,5}h/r} \tag{35a}$$
$$b_2 = a_{2,1} + a_{2,2}e^{a_{2,3}h/r} + a_{2,4}e^{a_{2,5}h/r} \tag{35b}$$
$$a_2 = a_{3,1} + a_{3,2}e^{a_{3,3}h/r} + a_{3,4}e^{a_{3,5}h/r} \tag{35c}$$

The parameters $a_{i,j}$ are collected in matrix $\mathbf{A}$:

$$\mathbf{A} = \begin{pmatrix} 1.9223 & -1.2524 & -0.8313 & 0.0055 & 6.1569 \\ 14.0826 & -11.0331 & -0.3656 & 0.0034 & 8.8199 \\ -0.2441 & -0.0639 & 2.8980 & 0.0441 & 3.3352 \end{pmatrix} \quad \text{for } 0 < h/r < 1 \tag{36a}$$

$$\mathbf{A} = \begin{pmatrix} 0.0748 & 0.3217 & 0.2720 & 0.2596 & 2.5328 \\ 0.2464 & 1.3197 & 2.5445 & 1.2137 & 0.3018 \\ 1.1736 & 0.0529 & 1.4179 & -1.5000 & -0.0018 \end{pmatrix} \quad \text{for } h/r < 0 \tag{36b}$$

The approximation factor f is compared with the numerically obtained values of $\Phi_{opt}(\tan\varphi \neq 0)/\Phi_{opt}(\tan\varphi = 0)$ in Figure 6. The purpose of f is to improve the accuracy of the axial induction computation when downwind convection is present, and this is clearly achieved. Also, the optimal Φ for tangential induction is matched well for $|h/r| << 1$. For $h/r \to 1$ and low downwind convection speeds, the analytical expression for $dw_y/dw_{0,y} \geq 1$ for angles $\beta < \pi/2$, so an approximation using Beddoes' approach is not possible.

In principle, an optimal Φ for the tangential induction would be necessary for accurate results. This would, however, increase the computation time in a way that is not reflected by the benefits of the increased accuracy considering the small importance of a precise tangential induction computation. Therefore, it is recommended to use the same approximation for Φ as for the axial induction.

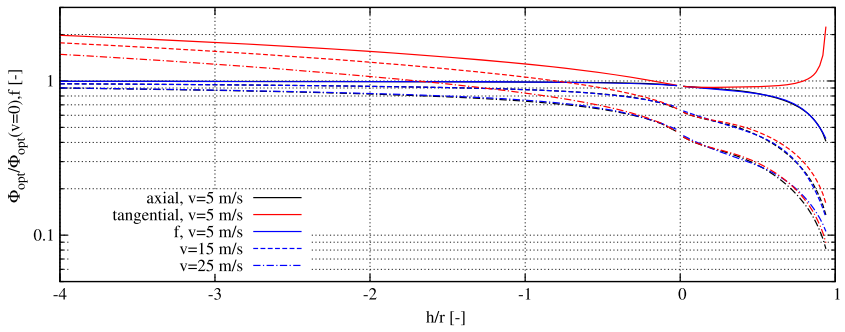

Figure 6. Comparison of the exact axial (black) and tangential (red) $\Phi/\Phi(v = 0)$ with the approximation factor f to the axial induction (blue), [cf. Equation (33)]. Results are shown for different convection speeds of 5 (solid), 15 (dashed) and 25 m s^{-1} (dash dotted). Vortices are trailed at $r = 10$ m; the rotation speed is $\Omega = 12.1$ rpm. The exact $\Phi/\Phi(v = 0)$ and the approximation factor f are almost identical, which is why the black lines are hidden behind the blue lines, except for positive h/r at high wind speed. The tangential induction results are fundamentally different. The functions are not evaluated at $h/r = 0$ and $h/r = 1$, where the optimal Φ without convection tends to zero and infinity, respectively.

5. DETERMINING THE COUPLING FACTOR

Because different operating conditions change the ratio of induction from the near and far wake, the coupling factor is not constant. An example for this is the operation of a turbine above rated wind speed. If the wind speed increases, the helical pitch angle increases. This has a bigger influence on the induction from the far wake than from the near wake; therefore, the coupling factor decreases.

Andersen[7] has proposed to compute the coupling factor beforehand for each turbine, as a function of tip speed ratio and thrust coefficient, but here, a different approach is suggested to avoid these preliminary computations: In each time step, in addition to the computation of the axial far wake induction with a thrust coefficient that is reduced by multiplication with the coupling factor, a second reference BEM induction with complete thrust coefficient and tip loss correction is computed. This reference BEM induction $a_{ref,QS}$ is the induction following from Equation (11) without application of a coupling factor but using the Wilson and Lissaman tip loss correction.[1] The objective is to choose a coupling factor so that

$$a_{ref,QS} = a_{FW,QS} + a_{NW}, \tag{37}$$

where quasi-steady values $a_{FW,QS}$ and $a_{ref,QS}$ of the far wake and reference induction are used to reduce slow changes of the coupling factor because of the different dynamic behavior of the BEM model and the coupled model. The near wake induction a_{NW}, computed by dividing the induced velocity computed by the NWM by the free wind speed, reacts faster than the far wake induction, and thus, the dynamic near wake induction is used for the computation of the coupling factor.

A new value for the coupling factor k_{FW} can be determined in every time step for each blade section with the goal of fulfilling Equation (37) as

$$k_{FW,j}^{i+1} = k_{FW,j}^{i} + \frac{a_{ref,QS,j} - (a_{FW,QS,j} + a_{NW,j})}{\partial a / \partial k_{FW}}, \quad \text{with} \tag{38}$$

$$\partial a / \partial k_{FW} = 3k_3 C_T^3 k_{FW}^2 + 2k_2 C_T^2 k_{FW} + k_1 C_T \tag{39}$$

where the subscript j indicates the blade section. A time lag with the same time constant as the near wake part of the dynamic inflow model used in HAWC2 is applied on the coupling factors to avoid introducing numerical instabilities. If these sectional coupling factors were used in the coupled model, the induction along the blade would reach the same distribution as with the BEM model with tip loss correction. Since one purpose of using the coupled model is to achieve an induction distribution because of the whole trailed vortex system including the tip vortex, an average coupling factor is used for the entire blade. In order to closely match the complete thrust of a BEM computation, the coupling factors are averaged weighted by the sectional thrust forces:

$$k_{FW} = \frac{\sum_{j=1}^{n} \left(k_{FW,j} T_j\right)}{\sum_{j=1}^{n} T_j} \tag{40}$$

Further, before averaging, a maximum for the sectional coupling factor of 1.0 and a minimum of 0.5 have been implemented, to limit the influence of sections close to strong trailed vorticity on the whole blade.

With the approach presented here, preliminary runs to determine the coupling factor can be avoided. The necessary additional computation time is very small, since the reference induction value is not subject to dynamic inflow or shed vorticity effects and is not used to calculate any aerodynamic forces or the velocity triangle.

6. RESULTS

In Section 6.1, the NWM is first compared with the induction following directly from the Biot–Savart law for the NREL 5-MW reference turbine,[14] to evaluate the improvement due to the modifications of the NWM. Cases with wind speeds above and below rated are investigated.

In Section 6.2, the effect of the modification of the trailing functions to remove the time step dependency of the steady induction is illustrated for an exemplary normal production case.

Finally, in Section 6.3, the coupled model is validated against a BEM model and full rotor CFD results from EllipSys3D[3] in steady conditions.

6.1. Comparison of NWM with induction from Biot–Savart law

The accuracy of the approximation of the induction from the near wake, Equation (17), by the modified NWM is investigated in steady cases in this section. Moreover, the induction according to helical vortices trailed from a three-bladed

turbine, equations (20) and (21), is compared with the results from the coupled model to evaluate the separation of the wake into a lifting line-type near wake and a BEM-based far wake.

6.1.1. Root correction.

The root correction is demonstrated for the NREL turbine in a normal operation case with $\Omega = 9.2\,\mathrm{rpm}$, uniform inflow with $v_\infty = 8\,\mathrm{m\,s^{-1}}$ and unpitched blades in Figure 7. The results have been obtained in the following way: The axial and tangential induction, as well as the vortex strengths, at sections distributed over the blade from a run of the coupled model with all modifications presented in this paper has been used as input for a numerical integration of Equation (17) over a quarter rotation. The result from this integration is then compared with the near wake induction using either the integral of Beddoes functions from zero to infinity, which is equivalent to $D_X + D_Y$ or the corresponding integral of the functions corrected for the root error, $D_{X,C} + D_{Y,C}$ (cf. Section 4.2).

The improvement clearly appears in Figure 7, where the results according to the Biot–Savart law are closer to the results from the NWM with root correction up to a blade radius of 35 m.

6.1.2. Convection correction.

The effect of the convection correction is investigated for two cases above rated wind speed, again based on the NREL 5-MW turbine. In these cases, the uniform wind speeds are $v_\infty = 15\,\mathrm{m\,s^{-1}}$ and $v_\infty = 25\,\mathrm{m\,s^{-1}}$, the turbine is rotating with its rated speed of $\Omega = 12.1\,\mathrm{rpm}$ and the blade pitch is 10.54° and 23.195°, respectively. The induction and vortex strength from the coupled model is this time used as input for the numerical integration of the induction from circular arcs and helical arcs, equations (3) and (17). In Figure 8, the induced velocities resulting from these integrations, denoted as 'exact near wake' and 'exact near wake, no convection', are compared with the near wake induction from the NWM, without and with the correction for downwind convection of the vortices. The difference between solid and dashed lines in Figure 8 is

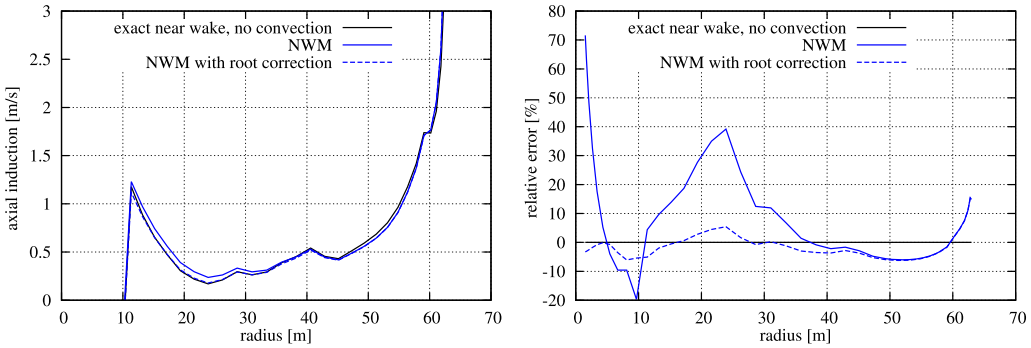

Figure 7. Effect of the root correction on the induction from the near wake for normal operation at $8\,\mathrm{m\,s^{-1}}$. Near wake induction (left) and relative error (right). NWM, near wake model.

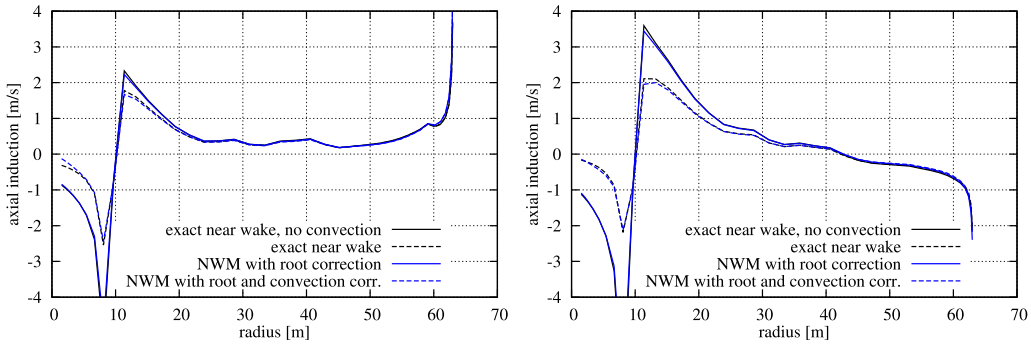

Figure 8. Steady near wake induction at 15 (left) and $25\,\mathrm{m\,s^{-1}}$ (right), NREL 5-MW reference turbine. The solid lines show the induced velocities according to numerical integration of the induced velocity due to circular vortex arcs, Equation (3), and according to the near wake model (NWM). The dashed lines are obtained by integration of the induced velocity due to helical vortex arcs, Equation (17), and the NWM with convection correction. Applying the correction of the downwind convection leads to almost the same difference in results as switching from circular to helical vortex arcs.

DOI: 10.1002/we

thus the difference between circular and helical vortex arcs for the exact results and the effect of the convection correction for the NWM results. The comparison shows that the convection correction can model the influence of the helix angle.

6.1.3. Assessment of separation in near wake and far wake model.

The purpose of this section is to evaluate how well the induction from near and far wake can be divided into an NWM-based and BEM-based far wake model. To investigate this issue, results from the coupled model are compared with the numerical integration of the induction from prescribed helical vortices trailed from a three-bladed rotor, based on equations (20)–(22). The trailed vortex strengths and convection speeds used as input in the prescribed helical vortex computations are the ones obtained with the coupled model computation.

The induction from these helical vortices can be divided into near wake induction of the blade concerned, which is the induction due to the vorticity trailed behind the blade during a quarter revolution. The far wake part includes the complete induction from the wakes of the other two blades and the far wake induction due to the wake of the blade concerned.

In Figure 9, the axial and tangential induction from integration of Equation (21) is compared with the results from the coupled model for wind speeds of 8 and 25 m s^{-1} and the corresponding rotational speeds and pitch angles as used in previous sections. Overall, the agreement of the near wake induction is better for the axial induction and lower wind speeds. The discrepancy in the tangential near wake induction at 8 m s^{-1} close to the tip is partly due to the minimum downwind convection in the helical vortex model that is not present in the coupled model. At the very tip, the disagreement at 8 m s^{-1} corresponds to 3% of the relative velocity. The tangential near wake induction at 8 m s^{-1} also shows a poor agreement at the mid-blade, because the convection correction is tuned to the axial induction only. At low wind speed, the optimal Φ for tangential induction is quite different from the optimal Φ for axial induction (cf. Figure 6).

The far wake induction is the result of two completely different models: a BEM model with reduced thrust coefficient and the prescribed wake vortex model with constant helical pitch and no wake expansion presented in Section 3. Even though the mean value of the far wake induction in the 8 m s^{-1} case is strongly depending on the limit of the downwind convection to a minimum of $2/3v_\infty$, the shape of the far wake induction can be used for qualitative comparison. Since the NWM cannot model the influence of the near wake from the two other blades, the far wake part of the coupled model has to account for both the far wake from all blades and the near wake from the other blades. The tangential induction predicted by the far wake part of the coupled model agrees remarkably well with the far wake and near wake of the other blades from the integration of the helical vortices, except an over-prediction of induction close to the root. At 25 m s^{-1},

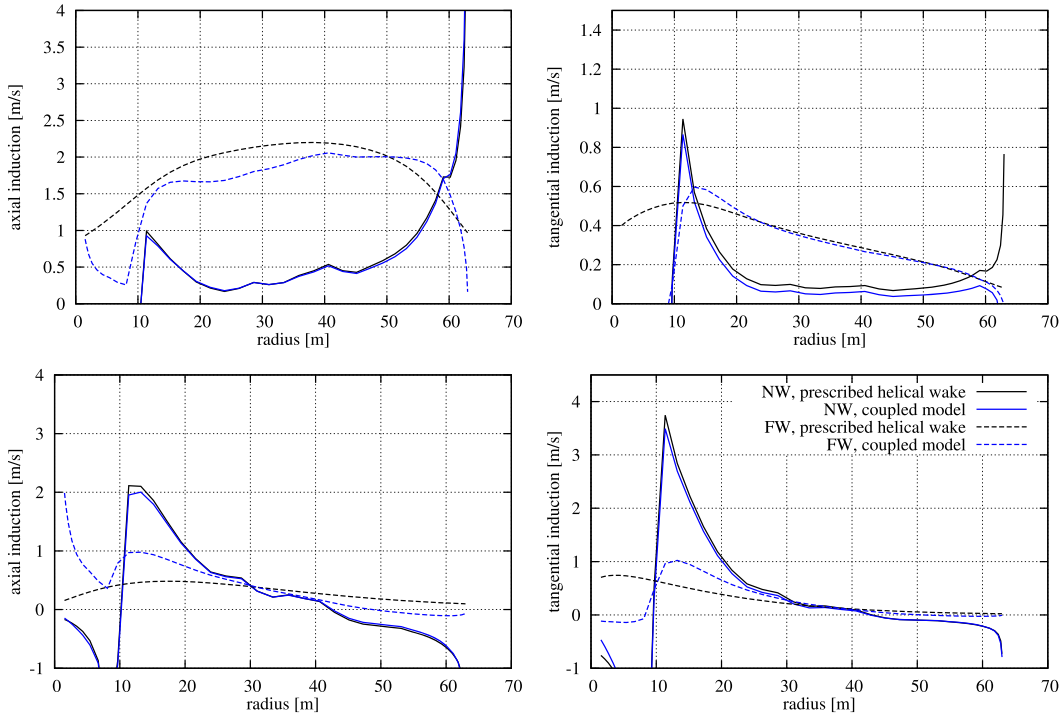

Figure 9. Near wake (NW) and far wake (FW) from three blades compared with Beddoes' near wake model with root and convection correction. Axial induction is shown on the left and tangential induction on the right side. The turbine operates at 8 (top) and 25 m s^{-1} (bottom).

the axial induction close to the root is over-predicted by the far wake part of the coupled model as well. At $8\,\mathrm{m\,s^{-1}}$, a comparison of the shape of the axial far wake induction shows too high induced velocities at the root and tip of the blade compared with the mid-blade sections.

Overall, the comparisons in Figure 9 show that radial distributions of the near wake and far wake inductions from the prescribed helical wake computations are qualitatively different, which indicates that the restriction of the NWM part to a quarter rotation is sufficient. The agreement of the near wake computations with results from the NWM is good except for tangential induction at the tip at $8\,\mathrm{m\,s^{-1}}$, which will only have a minor influence on the force distribution as the error is small compared with the tip speed and the loading at the tip is small because of the high axial induction. The far wake agreement between a BEM model and the prescribed helical vortex model is worse, which is expected because fundamentally different models are compared. The comparison shows, however, that a reasonable total induction distribution can be achieved by the coupled near and far wake model presented in this work.

6.2. Modified trailing functions

The modified trailing functions proposed in Section 4.1 make the steady induction from the NWM time step independent. This is illustrated in Figure 10, where the steady axial induction of the NREL 5-MW turbine at $8\,\mathrm{m\,s^{-1}}$ is shown for different time steps computed with the original trailing functions aside the induction predicted by the modified trailing functions. The result of the original model clearly converges to the result of the modified model if the time step is reduced. For commonly used time steps, mainly, the induction at the outer part of the blade deviates from the time step-independent result, but through the coupling factor (cf. Section 5), the whole blade is affected by a change in induction close to the tip. Note that the modification of the functions not only removes the need for a fine time step to achieve a good steady induction but also reduces the computation cost compared with the original model, as shown in Section 4.1.

6.3. Comparison of the coupled model with a BEM model and CFD

This section contains a comparison of steady-state power, thrust and radial load distribution predicted by the coupled near and far wake model, a BEM model and full rotor CFD. The results show that the steady states computed with the coupled near and far wake model are in line with those computed using established aerodynamics models. This is necessary if the coupled model is to be used in unsteady computations.

6.3.1. Steady power and thrust.

The thrust and power in steady operation of the NREL 5-MW reference turbine of the coupled model and a BEM model are compared for different wind speeds of 4 to $25\,\mathrm{m\,s^{-1}}$ in Figure 11, along with the coupling factor computed for the different cases. The power and thrust agree with deviations smaller than 1.5% and 2.5%, respectively. The coupling factor stays almost constant where the tip speed ratio and the helical pitch angle are fixed, and then gets reduced at wind speeds above rated. This can be explained by the faster convection of the wake away from the turbine at higher speeds and the corresponding bigger fraction of the induction due to the near wake.

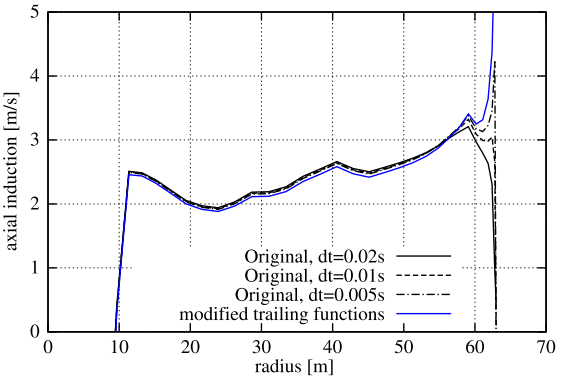

Figure 10. Results from the coupled model at $8\,\mathrm{m\,s^{-1}}$. The effect of the tip vortex varies with time step in the original model and converges to the time step-independent results of the modified model presented in Section 4.1.

6.3.2. Radial load distribution.

The radial in-plane and out-of-plane load distributions along the NREL 5-MW blade are shown in Figure 12 for normal operation at wind speeds of 8 and 25 m s^{-1}. The HAWC2 BEM model is compared with the coupled near and far wake model and full rotor CFD. The CFD results have been computed with the incompressible Reynolds-averaged Navier-Stokes (RANS) solver EllipSys3D[3] assuming fully turbulent flow and using the K-omega shear stress transport (SST) turbulence model by Menter to close the RANS equations. The computations are performed on a structured grid in which each blade exhibits 256 cells in the chord wise, 128 cells in the span wise and 128 cells in the normal direction. This results in approximately 14 million mesh cells for the entire rotor mesh.

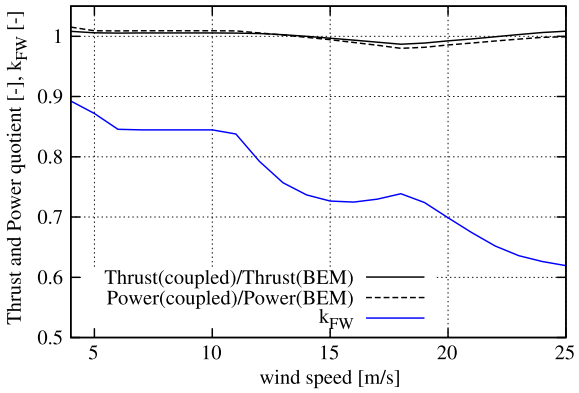

Figure 11. Agreement of power and thrust of coupled model with blade element momentum (BEM) model and the coupling factors automatically chosen for different wind speeds. The aerodynamic power of the NREL 5-MW rotor agrees within 2.5% and the thrust within 1.5%.

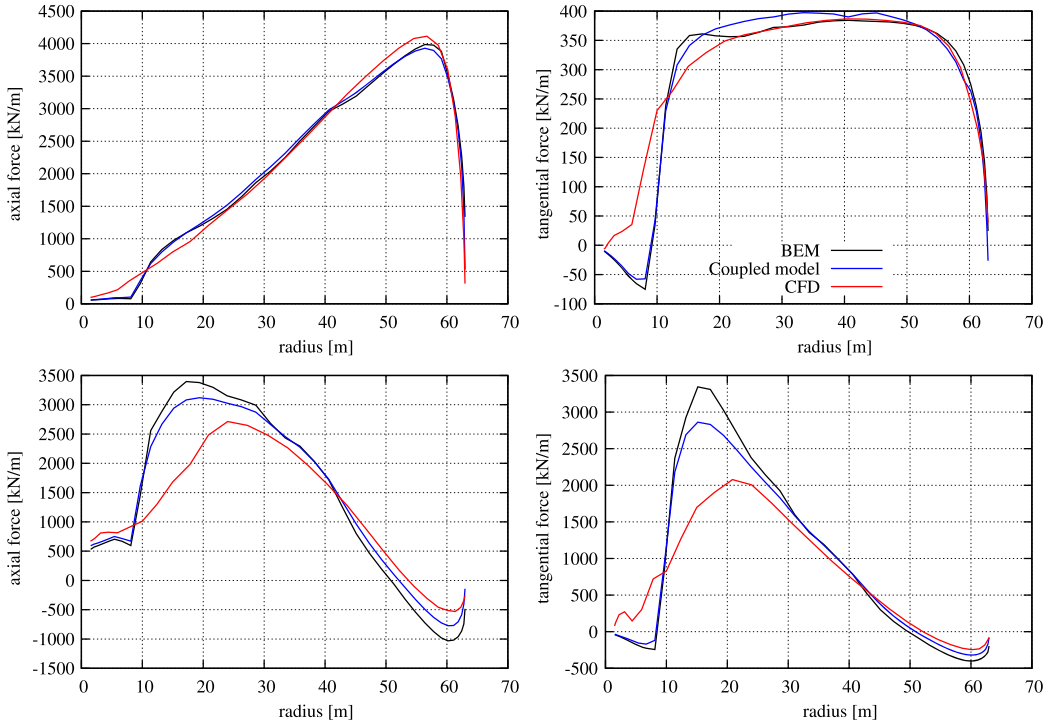

Figure 12. Comparison of axial and tangential forces in normal operation at 8 (top) and 25 m s^{-1} (bottom) of a blade element momentum (BEM) model, the coupled near and far wake model and full rotor CFD.

At 8 m s^{-1}, the thrust force agrees very well between all the aerodynamic models. There are some differences between the faster models and CFD close to the root and tip of the blade, which can be explained by the differences between the lift coefficients from the airfoil polars and the corresponding forces obtained in the 3D CFD computation. The differences seem to be largest for the thick DU airfoils used up to 19.95-m blade radius and the NACA64 airfoil with 17% thickness used on the outboard part of the blade.

The tangential forces are in close agreement between the models, with the coupled model over-predicting the tangential forces on mid-blade. Outboard of the root vortex and close to the tip vortex of the blade, the coupled model results are closer to CFD than the BEM results.

The forces from the CFD computations deviate strongly at 25 m s^{-1} wind speed for airfoils with more than 30% thickness up to a blade radius of 25 m, which is in agreement with the steady-state results at high wind speeds for flexible blades presented by Heinz.[15] The results from the coupled model clearly show the effect of the strong root vortex that is present in this case, and the loads are in between the BEM and CFD results. The CFD computation predicts a lower power output in the 25 m s^{-1} case than the other models. In operation, the blade pitch angle would be adjusted to reach rated power, which would improve the agreement of the loading at the inboard part of the blade. However, the comparison for exactly the same operation conditions shown here makes it easier to evaluate the differences between the models.

7. CONCLUSIONS

A hybrid aerodynamic model has been presented comprising a lifting line model for the near wake part of the trailed vorticity and a modified BEM model for the far wake. The improved modeling of steady and unsteady induction from the trailed vorticity is expected to make such a model better suited for aeroelastic simulations than a pure BEM-based model.

The NWM, based on a fast prescribed wake lifting line model by Beddoes, has been improved to be more efficient and to compute time step-independent steady results. The model has been modified in order to limit the wake length used in the induction computation to a quarter revolution, independent on the radial position where the vortices are trailed. Furthermore, the model has been extended to include the effects of downwind convection in the wake modeling, replacing the prescribed circular arcs used originally by helical arcs.

The thrust that the far wake induction computation is based on has to be reduced by a coupling factor to account for the near wake induction. This coupling factor, which has been a user input in previous implementations of the model, is now computed during the simulation.

It has been shown that the corrections presented in this paper improve the near wake induction computation and make it possible to achieve a good resolution of the tip induction without the need for lower time steps than what is commonly used in aeroelastic wind turbine codes. The results have been compared with numerical integration of the induction due to trailed vorticity behind a three-bladed rotor with good agreement. The correction for downwind convection has been found to be a necessary extension of the model to enable computations at high wind speeds.

The automated coupling factor computation has been shown to produce power and thrust levels close to the widely used BEM models. A comparison with full rotor CFD showed an improved agreement of the radial load distribution because of the added NWM at high wind speed.

The work presented here enables using a more accurate and faster trailed vorticity computation for dynamic aeroelastic wind turbine simulations while retaining similar steady power and thrust results to well-known BEM models in the full wind speed range. The dynamics of the model are expected to be an improvement compared with those of a standard BEM model. An ongoing validation of the dynamic behavior against a free wake vortex code will be published in the near future.

ACKNOWLEDGEMENT

This work was supported by the International Collaborative Energy Technology R&D Program of the Korea Institute of Energy Technology Evaluation and Planning (KETEP), granted financial resource from the Ministry of Trade, Industry & Energy, Republic of Korea. (No. 20138520021140)

REFERENCES

1. Wilson R, Lissaman P. *Applied Aerodynamics of Wind Power Machines*. Oregon State University: Corvallis, Oregon, 1974.
2. Madsen Aagaard H, Mikkelsen R, Sørensen N, Hansen M, Øye S, Johansen J. *Influence of Wind Shear on Rotor Aerodynamics, Power and Loads*, Forskningscenter Risoe. Risoe-R-1611: Denmark, 2007,101–116.
3. Sørensen N. General purpose flow solver applied to flow over hills. Ph.D. Thesis 1995.

4. Hansen MH. Aeroelastic instability problems for wind turbines. *Wind Energy* 2007; **10**: 551–577.
5. Beddoes TS. A near wake dynamic model. *Proceedings of the AHS national specialist meeting on aerodynamics and aeroacoustics*, Arlington, 1987; 1–9.
6. Madsen HA, Rasmussen F. A near wake model for trailing vorticity compared with the blade element momentum theory. *Wind Energy* 2004; **7**: 325–341.
7. Andersen P. Advanced load alleviation for wind turbines using adaptive trailing edge flaps: sensoring and control. Ph.D. Thesis 2010.
8. Wang T, Coton FN. A high resolution tower shadow model for downwind wind turbines. *Journal of Wind Engineering and Industrial Aerodynamics* 2001; **89**: 873–892.
9. Hansen MH, Gaunaa M, Madsen HA. *A Beddoes–Leishman Type Dynamic Stall Model in State-space and indicial formulations*. Risø-R-1354: Roskilde, Denmark, 2004.
10. Larsen T, Hansen A. *How 2 HAWC2, The User's Manual*, Forskningscenter Risoe. Risoe-R-1597: Denmark, 2007.
11. Kim T, Hansen AM, Branner K. Development of an anisotropic beam finite element for composite wind turbine blades in multibody system. *Renewable Energy* 2013; **59**: 172.
12. Larsen TJ, Madsen HA, Larsen GC, Hansen KS. Validation of the dynamic wake meander model for loads and power production in the Egmond aan Zee wind farm. *Wind Energy* 2013; **16**(4): 605–624.
13. Yde A. *HAWC2 wind turbine models*, 2014. http://www.hawc2.dk/HAWC2%20Download/HAWC2%20model.aspx (Accessed 14 March 2014).
14. Jonkman J, Butterfield S, Musial W, Scott G, *Definition of a 5-mw reference wind turbine for offshore system development.* Technical Report, National Renewable Energy Laboratory, 2009.
15. Heinz J. Partitioned fluid–structure interaction for full rotor computations using cfd. Ph.D. Thesis 2013.